

NeuSort: An Automatic Adaptive Spike Sorting Approach with Neuromorphic Models

Hang Yu, Yu Qi, *Member, IEEE*, and Gang Pan, *Member, IEEE*

Abstract—Spike sorting, which classifies spiking events of different neurons from single electrode recordings, is an essential and widely used step in neural data processing and analysis. The recent development of brain-machine interfaces enables online control of external devices and closed-loop neuroprosthetics using single-unit activity, making online spike sorting desired. Most existing spike sorters work in an offline manner, i.e., sorting after data collection. However, offline spike sorters usually suffer from performance degradation in online tasks due to the instability of neural signals. In an online process, neuronal properties can change over time (such as waveform deformations), and new neurons can appear. Therefore, a static spike sorter requires periodic recalibration to maintain its performance. This study proposes a novel online spike sorter based on neuromorphic models (NeuSort), which can adaptively adjust itself to cope with changes in neural signals. NeuSort can robustly track individual neurons' activities against waveform deformations and automatically recognize new coming neurons in real-time. The adaptation ability of NeuSort is achieved by online parameter updates of the neuromorphic model, according to the plasticity learning rule inspired by biological neural systems. Experimental results on both synthetic and neural signal datasets demonstrate that NeuSort can classify spiking events automatically and cope with non-stationary situations in neural signals. NeuSort also provides ultra-low energy cost computation with neuromorphic chips.

Index Terms—Spike sorting, Spiking Neural Network, Extracellular single-unit recordings

I. INTRODUCTION

Analysis of individual neuron activities plays a crucial role in neuroscience research [1]–[3]. Usually, extracellular recording with one electrode contains spike firing activities from several nearby neurons, and different neurons generate action potentials with diverse extracellular waveform [4]. One technique procedure called spike sorting aims to classify the activities of a single neuron based on the similarity of the waveform shapes. Then the single-unit activities can be utilized for further analysis in neuroscience.

Over the past decades, the emergence of large-scale neural recordings has proposed new requirements and challenges for spike sorting techniques. This trend witnessed a boom in the development of software and tools towards automatic

spike sorting, such as Osort [5], Kilosort [6], Klusta [7], MountainSort [8], HerdingSpikes [9], SpyKING CIRCUS [3], Wave_clus [10], IronClust [11], HDSort [12]. Typically spike sorting is applied after all the data are collected, and existing spike sorters are mainly employed offline.

A critical problem is that a spike sorter usually demonstrates lower online performance than offline sorting. While most approaches are template-fixed after the setting or training phases, it is possible for cells to drift over time and change their positions with respect to the recording probe. These drifts can introduce distortions of the waveforms, even appearances/disappearances of neurons themselves recorded extracellularly. The primary source is mechanical [13]: *in vivo*, attribute to the pressure release after the insertion of a probe, cells are likely to drift or rotate from initial positions. These perturbations can be slow and continuous. Due to the non-stationary property in neural signals and instability of signal recording [14], the waveforms of the same neuron can deform over time, which degrades the accuracy of spike sorting.

There is yet no consensus on how to deal with waveform deformations in extracellular recordings. Some efforts have been made in a template-matching based approach. One primary option is to correlate the incoming signal with known spike waveforms. [10], [15], [16] utilized discrete wavelet transform (DWT) to correlate the signal with existing waveform libraries. [3] combined density-based clustering and template matching into iterative steps, where masked the raw data with isolated waveforms in previous cycles. Another option is to perform a non-rigid spatial registration of the extracellular signals to estimate deviation. [13] obtained an average template of the mean of activity histograms computed by record chunk, which estimated the offset along the depth dimension of the electrodes of Neuropixels. In a follow-up study, [17] generalized probe drifts in three dimensions. Such delicate templates require manual interaction for calibration, and the spike waveforms of interest should be known a priori to the user.

For the purpose of handling deformations, one possible way is to introduce module plasticity to trace neurons online. In spiking neural networks (SNN), the artificial neurons communicate via spikes and synaptic inputs. With synaptic inputs from other neurons, the neurons temporally integrate, and they produce a spike when their accumulated membrane potential crosses a threshold. By employing models of synaptic plasticity, SNNs have been shown to be able to perform several complicated learning tasks [18]–[22]. Especially, [20] presented a neural algorithm for the rapid online learning and identification of odourant samples under noise on neuromorphic chips *loihi*.

Hang Yu is with the College of Computer Science and Technology, Zhejiang University, Hangzhou, China.

Yu Qi is with the Affiliated Mental Health Center & Hangzhou Seventh People's Hospital, and the MOE Frontier Science Center for Brain Science and Brain-machine Integration, Zhejiang University School of Medicine, Hangzhou, China.

Gang Pan is with the College of Computer Science and Technology, Zhejiang University, and with Zhejiang Laboratory, Hangzhou, China.

Corresponding authors: Yu Qi (qiyu@zju.edu.cn) and Gang Pan (gpan@zju.edu.cn).

Compared to traditional machine learning approaches to tackle the spike sorting problem [23]–[29], SNN-based solutions represent the intrinsic capability of functioning in real-time, and make them natural candidates for BCI applications.

In this paper, we propose NeuSort, an automatic spike sorting method based on neuromorphic computing. Since the waveform changes are continuous and tardy, a neuron can be adaptively tracked online by maintaining a waveform library tracing updates over time. Driven by plasticity learning rules, the neuromorphic model is updated online, where the spike signals can be processed sequentially to converge to a spike sorter automatically within a few minutes. Thus, it can serve as a plug-and-play module for online spike sorting and reduce human interaction. Besides, the online plasticity-driven model update enables an adaptive spike sorter by automatically adjusting the model following changes in spike waveforms. It traces waveform deformation in neural signals, which can perform stably given waveform changes, especially for long-term recordings. NeuSort improves the robustness against non-stationary neural signals with spike waveform deformation, thus enabling long-term stable online spike sorting. The proposed neuromorphic spike sorter has great potential for ultra-low-cost spike sorting applied to neuromorphic chips for implantable BCI devices.

The remainder of this paper is organized as follows. We present the structure of our method in Section II. The experimental results are reported in Section III. Discussion are probed in Section IV. Finally, conclusions are drawn in Section V.

II. THE NEUSORT METHOD

Figure 1 illustrates the framework of the NeuSort spike sorter for one channel, which follows the pipeline of spike sorting. Firstly, the raw neural signals are preprocessed, and spikes are detected as spike candidates. For classifying spike candidates, the encoding layer uses a receptive field encoder to transfer the waveform of spike candidates into spike trains. The encoding layer is fully-connected to the perception layer. The firing of nodes in the perception layer is based on spiking events, and the weights are learned with the Hebbian learning rule. Finally, the sorted spikes are output with timestamps. Note that the module presents in Figure 1 is for one single neural signal channel. For multiple channels, each channel contains an independent module.

Since *spikes* exists in both neural signals and spiking neural networks, we refer *spike* and *spike train* in the spiking neural network as *event* and *event train* in the following content.

A. Signal preprocessing

Three steps are included to convert the original raw data into spike candidates: filtering, spike detection, and realignment.

Filtering: The continuous multi-channel data is firstly band-pass filtered with a 3-order Butterworth filter. After this step, the low-frequency components of the signals are removed.

Spike detection: Then the spike candidates are detected. A nonlinear energy operator (NEO) is acted to capture changes in the energy of the signal. In discrete time, the NEO ψ on filtered signal S is defined as:

$$\psi[S(t)] = S^2(t) - S(t-1) \cdot S(t+1), \quad (1)$$

where $S(t)$ is the sample point of the t time waveform. Since a spike is characterized by localized high frequencies and an increase in instantaneous energy [30], the NEO is large only when input is both high in power and frequency (i.e., $S^2(t)$ is large while $S(t+1) \cdot S(t-1)$ is small). It is relatively simple to implement using a convolution kernel or a running window, occupies little computational overhead, and can be applied online. After detection, the spike candidate C consists of N data points.

Spike re-alignment: The purpose of spike alignment is to align each spike candidate C to the point of its maximum amplitude (in some cases, the maximum value of the spike candidate may be the minimum value of the waveform). To avoid spike misalignments attributable to low sampling [14], spike candidate maxima location is refined by using cubic spline-interpolated waveforms 5 times. After realignment, the waveforms are downsampled back to the length of the original points. Note that the peak of a waveform cannot be measured accurately because it only reaches for a concise period. Thus, the peak may fall between the time points at which the signal is sampled.

B. NeuSort: the neuromorphic model

A two-layer neuromorphic network is designed to transfer and assign the raw input candidates into classified clusters, as shown in Figure 1. The first layer is called the *encoding layer*, consisted of a group of sensor nodes. The following layer is the *perception layer*, composed of a set of Integrate-and-Fire (IF) output nodes.

1) *Encoding layer*: The encoding layer converts the spike candidate into a map of artificial event trains, encoding the shape of the waveform within the sliding window at each time step.

The Gaussian receptive field, as introduced in [31], allows the mapping of real-valued vectors into a sequence of events. The receptive field consists of a collection of sensor nodes with overlapping sensitivity scales. The intersection points with each Gaussian neuron are computed and translated into neuron events for one continuous value. One continuous value may activate multiple neurons in the field. Unlike [32], the indices of activated neurons in the field are preserved, while firing time is ignored.

A spike candidate, $C_t = [c_{t_1}, c_{t_2}, \dots, c_{t_n}]$, is the time point vectors from time t_1 to time t_n . Each input variable is encoded independently by a group of sensor nodes of M one-dimensional receptive fields. An interval $[I_{min}^{c_{t_n}}, I_{max}^{c_{t_n}}]$ is defined for each c_{t_n} . The event J of sensor node ϵ at time t and position (m, n) is:

$$J_{\epsilon(t, m, n)} = \mathbb{P}_{\mu, \theta}(c_{t_n}), \quad (2)$$

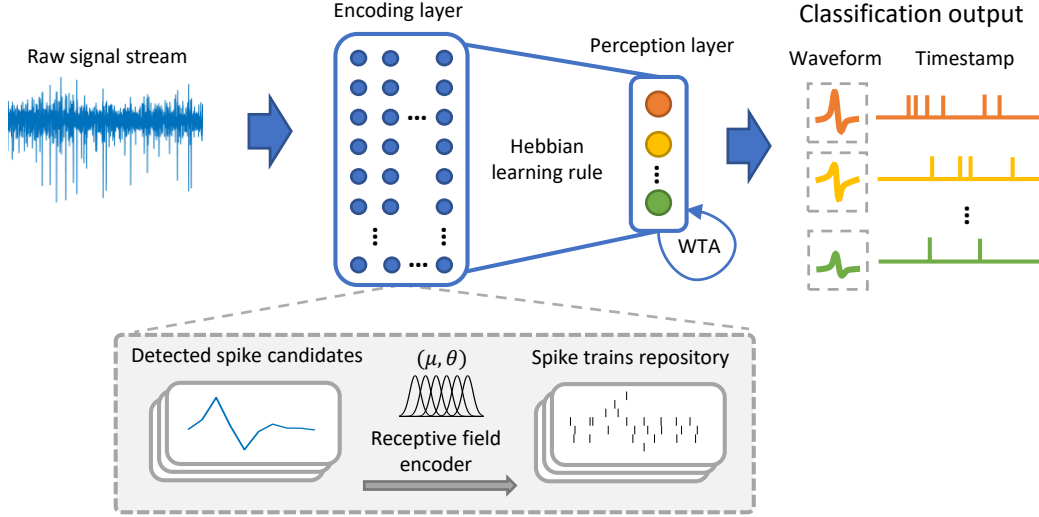


Fig. 1: The overview structure of NeuSort. The raw input signals are firstly preprocessed, then the spike candidates are detected for spike sorting. The encoding layer encodes the waveforms of spikes with a receptive field encoder into event training-based representations, which are fully connected to the perception layer. The perception layer distinguishes and assigns the input event trains into different nodes. Finally, spike trains are classified and output with exact timestamps.

where \mathbb{P} is the Poisson process of the Gaussian receptive field. The center μ_i of neuron i in Gaussian receptive field is calculated as:

$$\mu_i = I_{min}^{C_t} + \frac{2i-3}{2} \cdot \frac{I_{max}^{C_t} - I_{min}^{C_t}}{M-2} \quad (3)$$

and width θ :

$$\theta = \frac{1}{\beta} \cdot \frac{I_{max}^{C_t} - I_{min}^{C_t}}{M-2} \quad (4)$$

where $\beta \in [1, 2]$ controls the width of each Gaussian receptive field.

Within a brief period, the waveforms of spikes from the same neuron can be considered stationary. As the Poisson process is stochastic, the same input sequence may lead to slightly different outputs $I_{\epsilon(t,m,n)}$. With a well-designed receptive field, all outputs are roughly similar and can be clustered into the same class.

Receptive field coding is essential in distinguishing the waveform deformations and preventing the different cells from confounding. Ideally, the distance between the center of neighbor neurons is designed to be slightly larger than the deformation amplitude of adjacent input spikes. Thus, the distortion can be captured by both neighbor nodes in the receptive field and manifested as different weights connected to the next layer.

2) *Perception layer*: The role of this layer is to assign artificial input to different nodes corresponding to the waveforms of the biological neurons.

The output node ζ is an IF neuron, which membrane potential z at time t is governed by the following equation:

$$z_{(t,\zeta)} = \sum_n \sum_m^M J_{\epsilon(t,m,n)} \cdot \omega_{(t,m,n,\zeta)} \quad (5)$$

where $J_{\epsilon(t,m,n)}$ is the input event series from encoding layer, $\omega_{(t,m,n,\zeta)}$ is the fully connected weight from encoding layer to node ζ in perception layer. The classification output sequence is controlled by one predefined threshold th_d :

$$J_{\zeta(t)} = \Gamma(z_{(t,\zeta)}) \quad (6)$$

where Γ indicates the comparison between voltage z and threshold th_d . When z is greater than th_d , the output node fires an output spike.

C. NeuSort: online learning

The neuromorphic network update is based on the Hebbian learning rule, where neurons fired together should wire together [33]. Based on this bionic rule, the event activity which is stable over a period can be learned by the network, while the noise which contains no stable patterns will be ignored by the network. Specifically, as a waveform (encoded in artificial event trains) is input to the encoding layer, a group of specific nodes is activated together as the response. Using this rule, the weight $\hat{\omega}$ between two layers is updated with constant value τ_{h+} or τ_{h-} :

$$\dot{\omega}_{(m,n,\zeta)} = \begin{cases} \min(\omega_{(m,n,\zeta)} + \tau_{h+}, \omega_{max}), & \text{if in events,} \\ \max(\omega_{(m,n,\zeta)} - \tau_{h-}, \omega_{min}), & \text{else.} \end{cases} \quad (7)$$

As the waveform is repetitively presented, a certain group of nodes are repeatedly activated according to the Hebbian rule to "remember" the waveform pattern, thus learning to detect the waveform. The events can be sorted with a different group of neurons representing different waveforms. In this way, the NeuSort spike sorter can learn to sort the waveforms fully automatically, and all the signals pass through our network only once.

To ensure that each biological neuron is represented by only one node in the perception layer, a winner-take-all (WTA) mechanism is applied in the learning process. In our implementation, the node selection in the perception layer for a WTA mechanism is:

$$\dot{\zeta} = \max_{\zeta} z_{(t,\zeta)} \quad (8)$$

here $\dot{\zeta}$ is the selected node that is updated. If there is no selected node, the arrival spike will be randomly assigned to the neuron in the perception layer. Specifically, when one node is activated, other nodes are inhibited and will not be updated. The active node is the only node that reinforces its connection to learning the input pattern. Consequently, when a similar waveform segment occurs again, this node is the most likely to fire, thus reinforcing its response's specificity to this particular waveform pattern.

The WTA mechanism enables adaptive tracking of neurons against waveform deformation. As the waveform of a neuron deforms slightly, the corresponding node in the perception layer does not change, and the network updates itself to cope with the change in waveform patterns. When the waveform changes abruptly (usually indicating a new neuron occurs), a new node in the perception layer will be assigned such that new coming neurons can be detected automatically.

The learning process of the NeuSort network is specified as follows.

- The initial state: The output node studies the input waveform and distinguishes them. As event train input, no corresponding output node can be found. The WTA mechanism is not activated until the cumulative voltage of one output node exceeds the preset threshold. A randomly selected output node is updated and does not generate event output.
- The deformation state: The output node tracks the deformation neuron and updates itself. As event train input, the corresponding output node is selected by WTA and fires. The connection weights between two layers are updated with the Hebbian learning rule.

In our implementation, the output trains exactly correspond to the firing time of spikes in the input stream, while the output queues of other methods attach to vote the ownership of the input spikes.

The NeuSort spike sorter works in a fully automatic manner without supervision. As the unsorted spike waves are continuously input to the network, NeuSort gradually learns to converge to an effective spike sorter by *remembering* the repetitively occurring patterns (neuronal waveforms) with certain groups of nodes, by the synaptic weight update rule of the neuromorphic model. The synaptic update track and follow the changes in spike waveforms.

D. Criteria

Though there are plenty of methods, the agreement for the same high-density dataset is low, which are mainly false positives [34]. Comparing a sorting output to a ground truth, each spike can be labeled as:

- True positive (tp): Found both in the ground truth and the output.
- False Positive (fp): Found in the ground truth, but not in the output.
- False negative (fn): Found in the output, but not in the ground truth.

Moreover, the following performance measures are computed:

- Accuracy: $\#tp / (\#tp + \#fn + \#fp)$
- Recall: $\#tp / (\#tp + \#fn)$
- Precision: $\#tp / (\#tp + \#fp)$

Besides these classic assessments, a global F-score F across all ground truths and outputs is conducted as follows:

$$F = \frac{2 * H}{T + O}, \quad (9)$$

where T is the total number of ground truths, O is the total number of outputs, and H is the number of all outputs coinciding with the truths.

Utilizing the previous parameters, Equation 9 can also be rewritten as: $F = (2 * \#tp) / (2 * \#tp + \#fn + \#fp)$

III. EXPERIMENTAL RESULTS

Experiments are carried out to evaluate the performance of NeuSort in comparison with existing approaches, PCA-KM [35], Wave_clus [10], Osort [5]. We use synthetic and real neural datasets to evaluate the spike sorting performance under different conditions.

All the experiments implemented in MATLAB R2020a (Mathworks, Matick, MA) were run on a personal computer with Intel Core i5-10400 2.90 GHz CPU, 48G RAM.

A. Description of the datasets

A total of five benchmark datasets are employed in the experiments, including three synthetic datasets and two real neural signal datasets.

1) *Synthetic datasets*: We simulate different conditions of neural activities in the synthetic dataset to evaluate the performance of NeuSort. Specifically, we utilize three situations: Stable firing neurons, new coming neurons, and neurons with deformed waveforms.

- **dataset_syn1**. Synthetic dataset 1 (*dataset_syn1*) is constructed to test the performance of NeuSort in normal online situations. Following the methods in [10], [14], the waveforms are simulated with three neurons that fire at stable firing rates ranging from 1 to 10 Hz with a renewal Poisson process with a refractory period of 3 ms. For each neuron, one predefined and well-separated waveform is used and rescaled maximum value to $[-1, 1]$.
- **dataset_syn2**. Synthetic dataset 2 (*dataset_syn2*) is designed to evaluate the performance with new coming neurons. One neuron is chosen to be inhibited from firing for a period in the beginning, i.e., only two neurons fire during the training phase for method PCA-KM.
- **dataset_syn3**. Synthetic dataset 3 (*dataset_syn3*) contains a neuron whose waveform deforms slightly over time. We restrict the maximum deformation ratio of this neuron to

2, that is, the amplitude of the waveform is at most twice the initial value. During actual acquisition, we observe that the neural waveforms do not scale to such a large extent. Nonetheless, we enforce this property for better evaluations.

2) *Real datasets*: Two real neural signal datasets are used. The first real dataset contains multiple channels of neural signals recorded from a rhesus. The second dataset is an open dataset from a rat with the ground truth of one cell activity record.

- **dataset_real1**. The first real dataset is available from [36], [37], which provides only a single known ground truth neuron. The recordings are recorded from the CA1 hippocampal region of anesthetized rats, which contain the same neuron recorded both intracellularly and extracellularly. One example (dataset d553101) of the scaling of the ground truth waveform over time is found in the dataset, which can be caused by the distance shift between the extracellular probe and the neuron during the acquisition process. In Figure 5A, the ground truths are stained, ranging from cyan to magenta on the timeline. The first 100 spikes of ground truths (the left plot of Figure 5B) and the last 100 ones (the middle plot in Figure 5B) are identified easily as two neuron waveforms. From the perspective of waveforms, it is difficult to cluster the spikes of ground truths at various time points as the exact one.
- **dataset_real2**. Another real dataset contains neural signal data recorded with the Utah array (with 96 channels) from the motor cortex of a rhesus when performing a four-direction center-out task [38]. We use ten data segments recorded from different days (from 'MC01' to 'MC10'). Skilled sorters perform manual spike sorting to provide the label as the ground truth. All spike candidates and their timestamps are saved in .mat files, and the spike detection step is skipped on this dataset.

B. Experimental settings

Here we present the parameter settings of NeuSort as in Table I. All spike candidates are filtered with the passband located at [300, 3000]Hz and cropped to length $N = 64$.

TABLE I: Settings of NeuSort hyper-parameters

Parameters	Description	Value
I_{max}	The maximum of receptive field	200
I_{min}	The minimum of receptive field	-200
β	Field shape factor	2
d_r	Mean neighbor receptive field neuron distance	13
τ_{h+}	Short-term plasticity time presynaptic constant	0.2
τ_{h-}	Short-term plasticity time postsynaptic constant	0.1
th_d	Perception neuron firing threshold	3

For the receptive field, the boundary $[I_{min}, I_{max}]$ of input time points of spike candidates is set to $[-200, 200]$, and the field shape factor β is set to 2. The number of neurons M is normally specified manually. Here we dynamically calculate $M = (I_{max} - I_{min})/d_r$ through the bounds of field

$[I_{min}, I_{max}]$ and the distance d_r between receptive field neurons. We use $d_r = 13$, thus $M = \lceil (I_{max} - I_{min})/d_r \rceil = 31$.

For the network structure, the scale of the encoding layer is determined by the neuron number M of the receptive field, and the length N of input time trains, N varies according to different datasets. The scale of the perception layer is set to 9×1 . The encoding layer is fully connected to the perception layer, and the weights of synapses are initialized to 0.

For weight update, Hebbian learning rules apply on the synapses stemming from the encoding layer to the perception layer for each synaptic spike occurrence. We use the parameters $\tau_{h+} = 0.2$ and $\tau_{h-} = 0.1$ as plasticity constants for presynapses and postsynapses, separately. The firing threshold th_d of the perception layer is set to 3.

Diverse learning rate ratios affect the final effect of classification. As the ratio increases, the performance increases, and the rate of increase slackens. Under the fixed waveform, the higher τ_{h+} (which means a higher ratio) means a faster learning rate, which allows the network to identify the waveform faster. However, a sharp learning ratio does not significantly improve the recognition accuracy and causes the neurons in the perception layer to solidify too quickly, resulting in over-clustering. We try different combinations of ratios of parameters on a synthetic dataset. The influence of parameters on the recognition accuracy is given in Figure 2. The slope begins to slow down around 1.7 on the abscissa. Considering the recognition speed and accuracy, we finally choose the parameters $\tau_{h+} = 0.2$ and $\tau_{h-} = 0.1$.

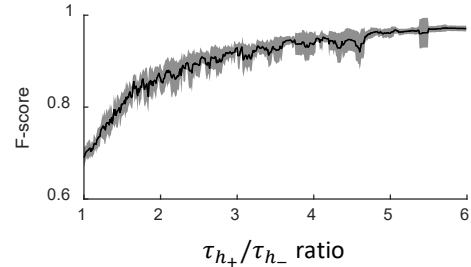


Fig. 2: Evaluation of the influence of parameter τ_{h+} and τ_{h-} .

C. Analysis of the learning process

We validate the performance of NeuSort by tracing the synapse weights of the model during one learning process, both in the initialization stage and the online adaptation of waveform changes. In this experiment, two well-separated neurons are utilized as ground truths, which are fired about 2000 epochs in a random order (each neuron fires about 1000 epochs). One neuron fires stably from beginning to end, and one neuron deforms its waveform linearly since the 1000 epoch.

1) *The initial learning process*: Firstly, we examine the plug-and-play learning process of NeuSort. As shown in Figure 3A, the first row illustrates the spike waveform at each epoch step (referred to as time t), and the second row illustrates the synapse weight map ω . The weights are initialized to zero. As the model receives the same waveform

repeatedly, the pattern gradually emerges in the synapse. At about epoch 200th, the model has learned the waveform.

Since the weight map updating is triggered by the appearance of spikes, a neuron with higher firing rates requires a lower time cost for spike sorter training. Figure 3D shows the time required for obtaining a stable sorter under different firing rates. NeuSort mainly converges in less than 100 seconds. Since the process is fully automatic without supervision, it can be used as a plug-and-play pipeline for online spike sorting.

2) *Online adaptation with deformation waveforms*: In Figure 3B, we investigate the online adaptation ability with waveform deformations. As shown in the first row, the spike waveform deforms since epoch 1000th. In the second row, the corresponding synapse weight map well tracks the changes in the waveform over time.

With slow and continuous deformations in the waveform, the same neurons in the perception layer are activated due to the overlap between adjacent receptive field neurons. Thus, the neurons learn to follow the change of waveforms, and the weights corresponding to the deformation spikes are updated (weight maps from epoch 1200th to 1800th). Results demonstrate that NeuSort can be adaptive to online waveform deformations, which can improve the robustness in long-term spike sorting tasks.

In Figure 3C, we present the final synapse weight map after the initial learning and online adaptation. Only two out of nine weights (weight 4 and 8) contain obvious meaningful spike patterns, indicating two different neurons in the channel. With the WTA strategy, the network is well-regulated and tends to use only one synapse weight map to represent a waveform pattern. The 'blank' synapse weight maps are preserved so that new coming waveforms can be captured.

D. Performance on the synthetic datasets

Three synthetic datasets are utilized to measure the performance of NeuSort with different conditions: 1) stable spike waveforms, 2) new coming neurons, and 3) spike waveform changes in time.

1) *Methods in comparison*: Comparison is carried out with three representative approaches of PCA-KM [35], Wave_clus [10], Osort [5].

- **PCA-KM**: As a classical spike sorting approach, PCA-KM uses principal component analysis (PCA) and K-means separately for feature extraction and clustering. Since the initial PCs are set up from data, we divide part of the data as the training set. Attribute to the number of clearly distinguishable neurons in a channel that did not exceed three [39], we decide $K = 3$ in the following tests.
- **Wave_clus**: A spike-sorting algorithm uses wavelet decomposition to extract features of the spike waveforms and superparamagnetic clustering (SPC) to cluster the spikes in this feature space. For comparison, we substitute PCA as a feature extraction method and fix the temperature parameter T in SPC for online running.
- **Osort**: This algorithm utilizes valley-seeking clustering and has a good accuracy-complexity tradeoff. Osort

provides source code for testing. Thus, we use the code with the parameters recommended in their article. Some of its detection parameters are modified to achieve better performance.

We evaluate the spike sorters in a pseudo-online manner where the spike waveforms are sequentially sent to spike sorters. For PCA-KM, a training set containing stable spike waveforms is used for parameter calibration. For Wave_clus, Osort, and NeuSort, no training is required.

The results are presented in Figure 4 and Table II. In Figure 4, the first column sketches the condition of three different synthetic datasets. The second column specifies the ground truth label for spike sorting, with one color representing one neuron (blue as 1, red as 2, yellow as 3). For visualization convenience, the spike waveforms are decomposed by PCA, and the first two components are plotted. Rest columns present the spike sorting results of different spike sorters. In each subfigure, dots with bright colors refer to a correct detection, while those with light colors are incorrect or missed detection.

2) *Performance with stable waveforms*: With *dataset_syn1*, where the spike waveforms are primarily stable, all the spike sorters achieve high performances. It can be seen from the ground truth that all the detected spikes are correctly stained, and only a few spikes far away from their cluster center are not detected or incorrectly stained. Specifically, the accuracies are 93.17%, 95.85%, 95.02%, and 94.51% for PCA-KM, Wave_clus, Osort and NeuSort respectively; the recalls are 95.86%, 98.82%, 96.81% and 96.35% respectively; and the precisions are 97.07%, 96.96%, 98.08%, and 98.01% respectively. Results show that all sorters can distinguish three different neurons, and NeuSort shows high statistical performance for online spike sorting.

3) *Performance with new coming neurons*: We evaluate the performance with new coming neurons with *dataset_syn2*. As shown in Figure 4, neuron 3 occurs later in the neural signals. The PCA-KM method, where the parameters are fixed after training, fails to detect neuron 3 since the neurons are not presented in the training phase. Thus, although PCA-KM works well in an offline manner, the online performance degrades due to minimal online adaptation ability, and only two valid neurons are correctly detected. The new coming neuron is correctly detected with Wave_clus, Osort, and NeuSort. Specifically, the recalls are 72.23%, 93.93%, 97.64%, and 96.85% for PCA-KM, Wave_clus, Osort, and NeuSort, respectively; and the precisions are 78.79%, 94.38%, 97.45% and 97.30% for PCA-KM, Wave_clus, Osort, and NeuSort, respectively. Results show that NeuSort can cope with new coming neurons in online spike sorting tasks.

4) *Performance with waveform deformations*: In online experiments, probe drift or cell distortion can cause slight changes in the spike waveforms of a neuron. As hinted in Figure 4 (the third row), the waveform of neuron 2 changes in time. Usually, the waveform deformation causes a performance decrease due to fixed decoders. All four sorters capture three valid neurons. With the PCA-KM method, only 53.53% of the spikes of neuron 2 are detected, and the missing detections are mainly after the waveform deformation. Thus, PCA-KM obtains a low accuracy of 70.69% with *dataset_syn3*. With

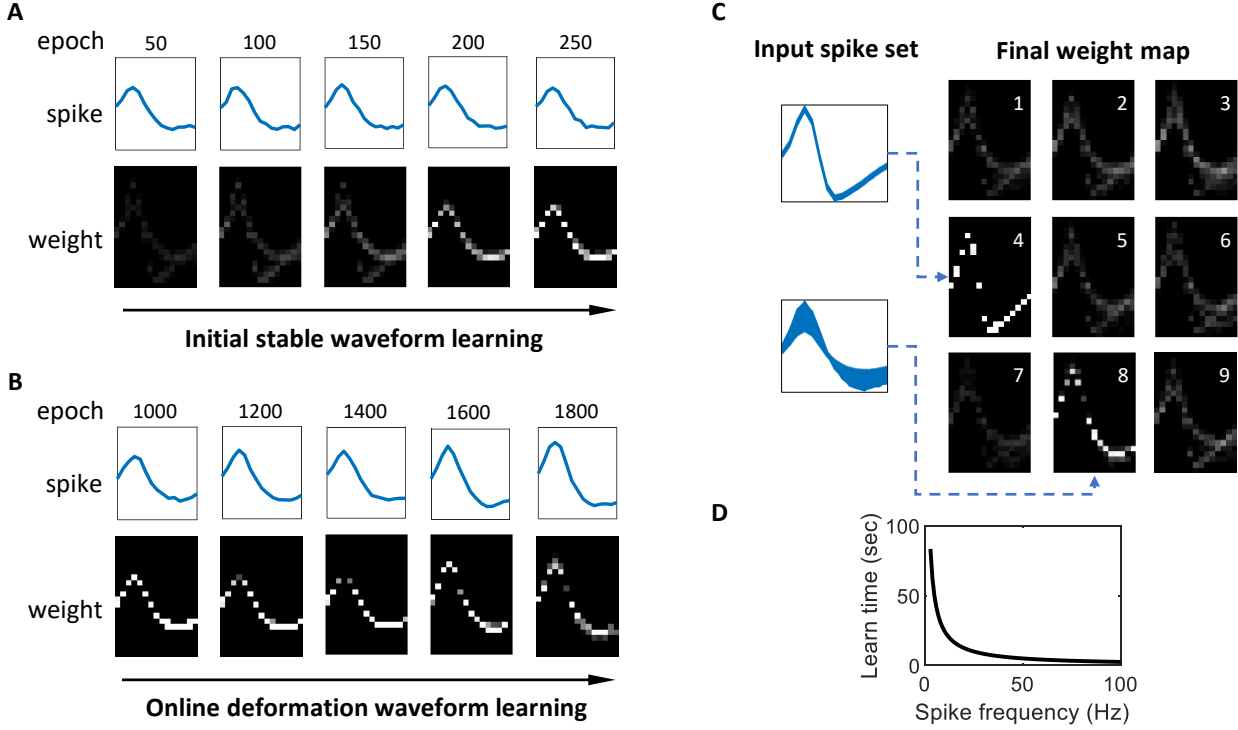


Fig. 3: The learning process of NeuSort. (A) The learning process with steady waveforms. (B) The automatic tracing with deformation waveforms. (C) The learned weight maps of the network. (D) Time of convergence against the firing rate of neurons.

TABLE II: Performance with the synthetic datasets

Dataset	Criterion	Method			
		PCA-KM	Wave_clus	Osort	NeuSort
dataset_syn1	Valid neurons	3	3	3	3
	Accuracy	0.9317	0.9585	0.9502	0.9451
	Recall	0.9586	0.9882	0.9681	0.9635
	Precision	0.9707	0.9696	0.9808	0.9801
dataset_syn2	Valid neurons	2	3	3	3
	Accuracy	0.6047	0.8895	0.9521	0.9431
	Recall	0.7223	0.9393	0.9764	0.9685
	Precision	0.7879	0.9438	0.9745	0.9730
dataset_syn3	Valid neurons	3	3	3	3
	Accuracy	0.7069	0.7759	0.7944	0.8544
	Recall	0.7380	0.8171	0.8377	0.9882
	Precision	0.9437	0.9389	0.9389	0.9449

Wave_clus and Osort, the waveform deformation is difficult to capture, where only 69.50% and 44.17% of the spikes are detected for neuron 2. NeuSort achieves the best performance under this condition, tracing 89.35% of the spikes of neuron 2. The accuracy of NeuSort is 85.44%, which is 7.85% and 6.00% higher than Wave_clus and Osort, respectively. Results demonstrate that NeuSort can effectively cope with waveform deformations to improve the robustness of online spike sorting.

E. Performance on the real datasets

We evaluate the performance of NeuSort with two real datasets: one single channel with intracellular recording and one multi-channel neural data over different days. Similar to

the simulation experiments, all the spike sorters are evaluated in a pseudo-online manner. A training set containing spike candidates is used for parameter calibration for PCA-KM.

1) *Performance with single probe intracellular recordings:* We evaluate the performance of NeuSort in the condition of waveform deformation in the real dataset. The dataset contains one intracellular cell record, which can be considered the ground truth. As shown in Figure 5A, the ground truths are stained, ranging from cyan to magenta. Through intracellular records, all ground truths should be gathered into one cluster. Nonetheless, it can be observed that the ground truths on different periods exhibited separate properties (the cyan and magenta spikes in Figure 5B).

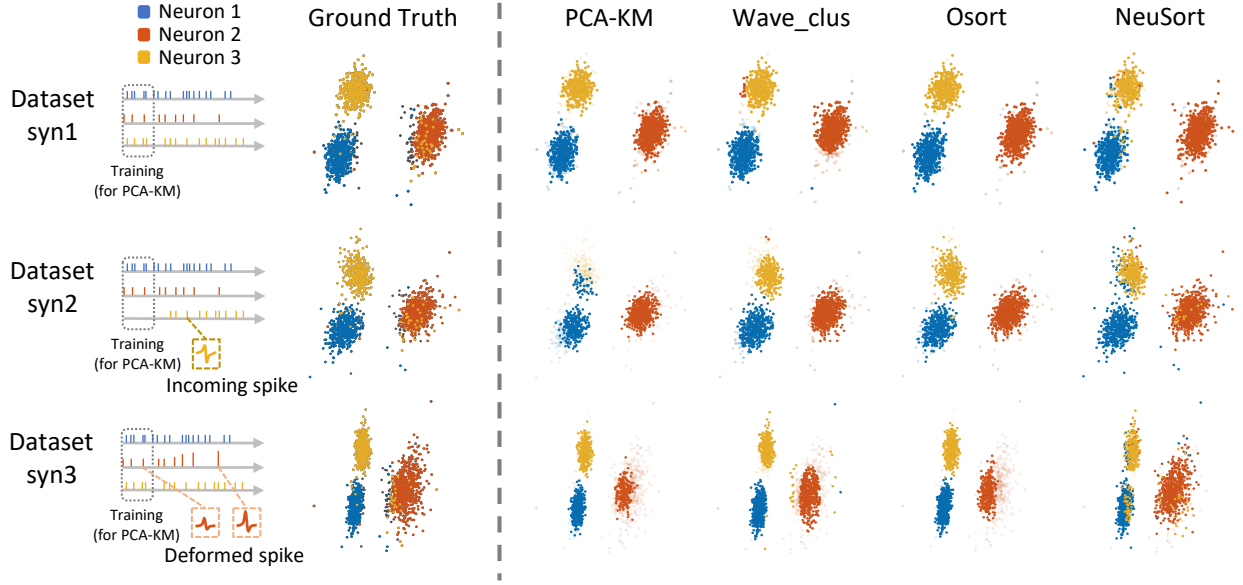


Fig. 4: Spike sorting performance with synthetic datasets.

The spike sorting performance is evaluated with F-score. By definition, the F-score of ground truth is 1. As shown in Figure 5D, all four sorters yield high spike sorting performance in the initial spikes. Specifically, the F-scores are 0.82, 0.96, 0.77, and 0.93 for PCA-KM, Wave_clus, Osort, and NeuSort, respectively. As the spike waveform gradually changes in time, the static spike sorters, such as PCA-KM, lose the neuron's track. Specifically, in the last part of the recording, the F-score of PCA-KM becomes 0. With the waveform deformation situation, NeuSort maintains a high F-score of 0.79, which is 0.31 and 0.16 higher than Wave_clus and Osort, respectively.

Figure 5C illustrates the spike detection results of different spike sorters of a segment at the end part of the recording. Results show that NeuSort can correctly capture the neuronal firing behaviors and perform better than other methods.

2) *Results on multi-day collections:* Here we evaluate the NeuSort with a larger real dataset recorded by Utah arrays (96 channels) from multiple days (MC01 to MC10). Again, experienced experts performed manual spike sorting to serve as the ground truths. Figure 6A illustrates the average waveforms detected by NeuSort for each channel in dataset MC01. The channel placement is depended on the placement of the Utah array. There are one or two putative neurons for most channels, while there are also several channels containing no neurons or three neurons.

The quantitative comparison of spike sorting performance is given in Figure 6B and Table III. Overall, NeuSort gains the highest median on accuracy and precision. Specifically, Osort, Wave_clus, and NeuSort obtain average accuracies of 77.40%, 75.26%, and 78.69%, respectively and precisions of 86.84%, 84.13%, and 88.98%, respectively. Four sorters show similar mean recalls of 84.96%, 86.51%, 87.27%, and 86.33% for PCA-KM, Wave_clus, Osort, and NeuSort, respectively.

Though PCA-KM is an automatic process of imitating the manual operation of experts, the input spikes are only judged

and classified according to the distance from each cluster center during the online procedure. As a result, some spikes with large variances are hard to recognize correctly. Therefore, K-means are not as good as the other three sorters on these criteria. PCA-KM only showed the best performance on MC3, indicating that the neurons firing in this segment are stable during acquisition. Other sorters' results are also better on MC3 than other data segments.

In this multi-channel dataset, NeuSort obtains the highest mean accuracy of 78.69% and mean precision of 88.98%, outperforms other comparing sorters, and shows high performance in processing large amounts of data.

F. Comparison of computational cost

It is essential that the computational time of spike sorting should be less than the duration of the recording. Otherwise, it is hard to complete spike sorting preprocessing and move on with downstream analysis [40], especially in closed-loop BCI decoding [41], [42]. We analyze the computational cost of the different sorters by examining *dataset_syn1* with 10-fold. 1500 spike samples are leveraged, and only the operation time is recorded. The result is shown in Figure 7.

Among these four sorters, PCA-KM, Osort, and NeuSort consume the linear computational time of 0.74, 4.55, and 5.82 seconds separately as the number of samples increases, while PCA-KM costs the shortest time. With the Wave_clus approach, the computational cost increases exponentially as the spike number increases since the sorting process computes with all the historical data. The calculation time reaches 58.35 seconds to classify all the samples.

NeuSort costs slightly higher than Osort because NeuSort takes more time to encode the original input into the spike series. The property of NeuSort in linear growth of computational time reveals the ability for long-term online sorting.

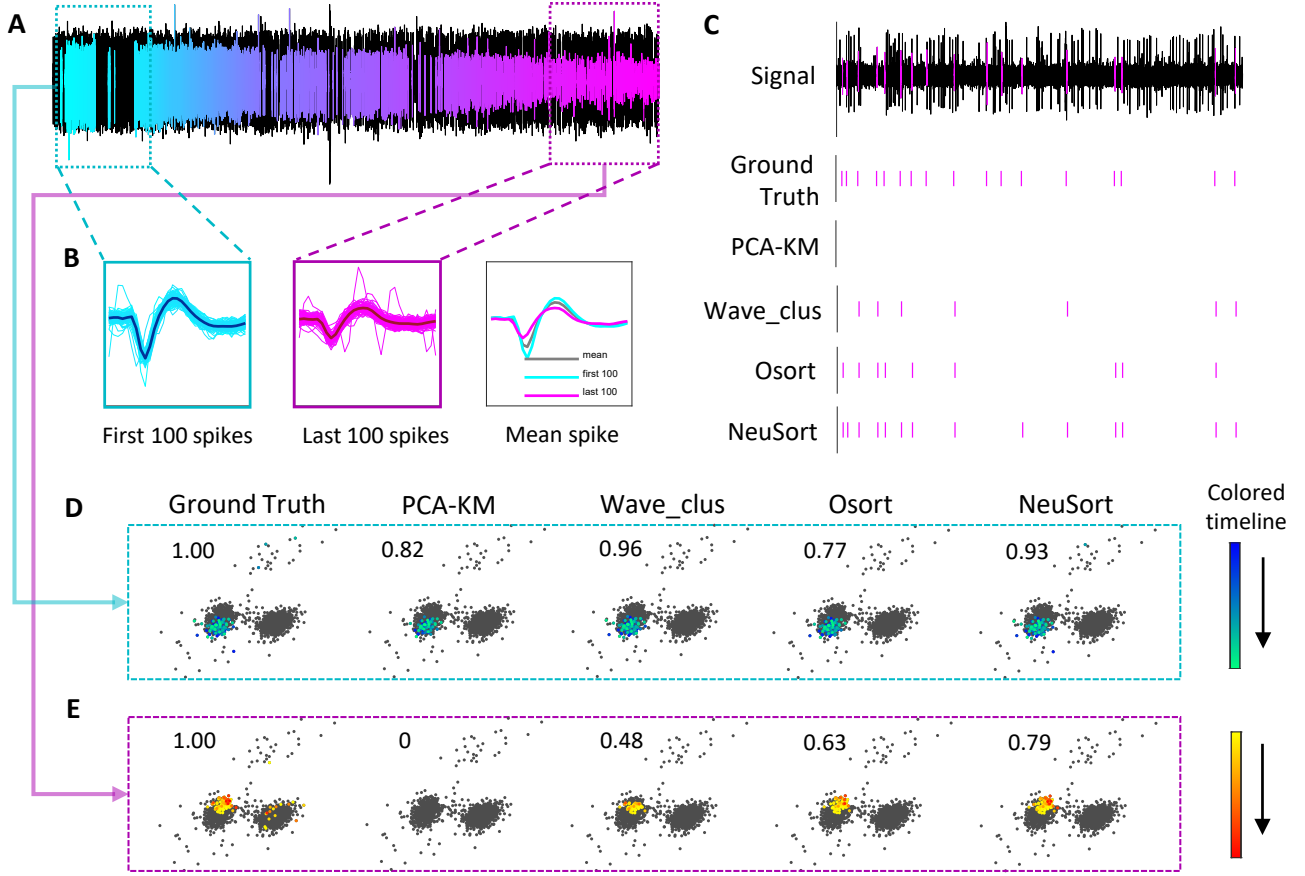


Fig. 5: Performance with dataset_real1. (A) The ground truths acquired from intracellular recordings, stained with colors from cyan to magenta. (B) The first 100 spikes and the last 100 spikes are plotted in cyan and magenta, respectively. The average waveforms of all spikes, the first and last 100 spikes, are illustrated. (C) One segment of spike sorting results of different methods. (D) & (E) Spike sorting results of first and last 100 spikes. The spiking events are stained by different colors over time, as shown in the colorbar on the right. The values on the top-left indicate the F-scores.

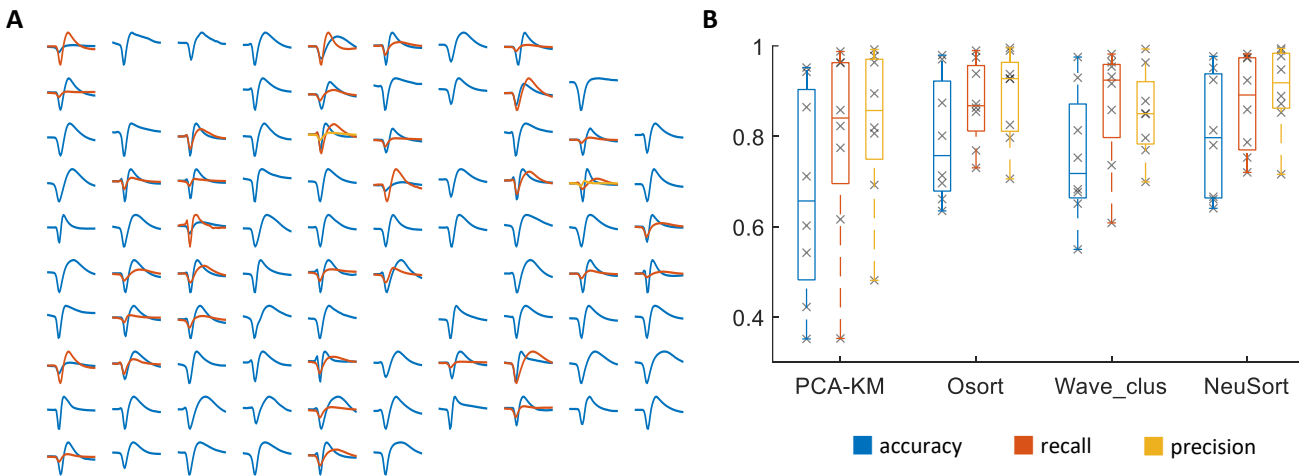


Fig. 6: (A) Average waveforms detected on neural signals recorded by a 96-channel Utah array. (B) Performance comparison with boxplot on dataset_real2.

TABLE III: Performance comparison with dataset_real2

Dataset	PCA-KM			Wave_clus			Osort			NeuSort		
	Accuracy	Recall	Precision	Accuracy	Recall	Precision	Accuracy	Recall	Precision	Accuracy	Recall	Precision
MC01	0.9425	0.9636	0.9774	0.9753	0.9820	0.9931	0.9795	0.9896	0.9897	0.9768	0.9823	0.9942
MC02	0.5421	0.6158	0.8191	0.6507	0.7358	0.8490	0.6347	0.8632	0.7057	0.6404	0.8589	0.7157
MC03	0.9521	0.9876	0.9636	0.9296	0.9637	0.9633	0.8739	0.9385	0.9270	0.9514	0.9727	0.9775
MC04	0.7112	0.8579	0.8061	0.7525	0.9318	0.7963	0.6961	0.7300	0.9375	0.7803	0.7864	0.9900
MC05	0.4218	0.7743	0.4809	0.5494	0.6081	0.8507	0.7131	0.8716	0.7968	0.6660	0.7528	0.8523
MC06	0.6021	0.8225	0.6920	0.6825	0.8582	0.7692	0.6609	0.7686	0.8251	0.6605	0.7199	0.8890
MC07	0.8643	0.9621	0.8947	0.6761	0.9542	0.6988	0.9704	0.9745	0.9957	0.9248	0.9747	0.9476
MC08	0.8076	0.8502	0.9417	0.8140	0.9363	0.8617	0.7918	0.8293	0.9460	0.8258	0.8391	0.9811
MC09	0.4470	0.6817	0.5648	0.5842	0.7773	0.7016	0.4854	0.7026	0.6110	0.4998	0.7611	0.5928
MC10	0.9322	0.9801	0.9502	0.9116	0.9795	0.9293	0.9344	0.9833	0.9495	0.9437	0.9850	0.9574
mean	0.7222	0.8496	0.8090	0.7740	0.8651	0.8684	0.7526	0.8727	0.8413	0.7869	0.8633	0.8898

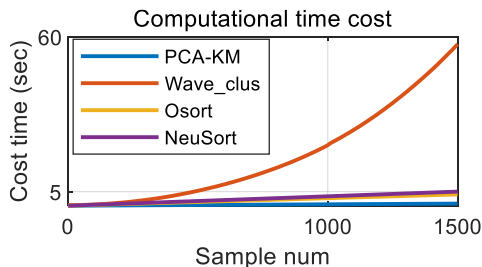


Fig. 7: Comparison of computational costs.

G. Power consumption estimation

Theoretically, the proposed SNN structure has one key benefit of high energy efficiency and ultra-low-cost on neuromorphic chips. Therefore, we conduct a power consumption estimation based on the previous work of such neuromorphic hardware.

Referring to [43], we assume that the energy emitted by one spike is α . During the phase of online recognition, we measure 41 spikes for processing a single input waveform in *dataset_real2* on average, and the number of inputs per second is 3.42×10^3 . Thus, the energy consumed for processing each channel is $1.4 \times 10^5 \alpha$. Multiplying this energy by the channel number of 96, the total power requirement P is:

$$\begin{aligned}
 P &= 1.4 \times 10^5 \alpha \text{ Watts/channel} \times 96 \text{ channel} \\
 &= 1.34 \times 10^7 \alpha \text{ Watts}
 \end{aligned} \tag{10}$$

Corresponding to two published spike-based neuromorphic circuits Loihi [44] and Neurosynaptic core [45], the single spike energy α of two circuits are 23.6 and 45.0 pJ separately. The power consumptions are 0.317 and 0.605 mW using the formula in Equation 10.

IV. DISCUSSION

A. Comparison of existing SNN methods

As an emerging strategy for spike sorting, there are several pioneers in resolving with SNNs.

[46] introduced a 2-layer SNN implementation in real-time. 32 frequency band-pass filters decomposed the input data, which the outputs modulated the firing of the corresponding

input neurons. 32 input LIF neurons were connected to each other with inhibitory synapses to implement a winner-take-all strategy, and were fully connected to 5 output LIF neurons. The synapses were trained through spike-timing dependent plasticity (STDP). In another case, [47] proposed a 3-layer SNN implementation for spike sorting from single channel recording and tetrode data. The input neuron layer encoded the waveform shapes of spike candidates. The intermediate hidden layer was used to learn various waveform fragments from the input neuron layer via plasticity rules. The output layer learned the combination orders of different fragments from the hidden layer as different units and to output the spike trains. Overall, an attention neuron gated the network learning only when an action potential occurrence was detected.

These two SNN-based solutions can both handle real-time data streams. However, the synapses are fixed in these scenarios. Since the training and operating phases are separated, the synapses have no dynamic capabilities for learning waveform deformations online.

Similar to [47], we treat the candidate input spikes as graphs. The difference is that, all inputs go through the network only once, instead of multiple looping. Observed from a short period of time, the waveforms of the same neuron are stable, so the effect of similar input multiple times could be regarded as repeated activation of the same feature.

B. Advantage of neuromorphic chips

A potential advantage of the NeuSort approach is the ultra-low computational cost of implementing neuromorphic chips. With the large-scale neural recording requirements, how to transmit such a large amount of data through limited bandwidth has become a recent bottleneck. Performing a spike sorting directly before signal transmission, which only transmits the sorted spikes, can vastly decrease the transmission cost. Nerve neurons, however, are pretty sensitive to temperature. A tiny increase in temperature (Less than 1°C) can cause cell degeneration, in a possibly non-reversible manner, which challenges the power consumption of hardware. To solve this, the spike sorter should be computed at a low cost to be implemented on an implantable device.

The neuromorphic architecture has a natural advantage in power consumption. The characteristic of timing of neuromorphic architecture is asynchronous, which only consumes

energy in operating spikes. Besides, unlike the organization of separate computation and memory in traditional Von Neumann architecture, a collocated processing and memory design makes neuromorphic chips more efficient and occupies less space. The NeuSort approach based on neuromorphic chips provides an ideal solution to realize such intracranial BCI devices. The number of applications of such networks remains limited. This study showed encouraging results on neuromorphic model-based applications to spike sorting.

V. CONCLUSION

In this paper, we proposed NeuSort, a novel automatic adaptive spike sorting approach based on neuromorphic models. With the characteristics of neuromorphic models, NeuSort can learn to sort spike waveforms in an unsupervised way and adaptively adjust the spike sorter to cope with new coming neurons and the deformation of waveforms. Experimental results with real data showed that NeuSort achieved state-of-the-art performance with low computational costs. The results strongly demonstrate the potential of a neuromorphic model-based spike sorter for ultra-low-cost spike sorting applied to neuromorphic chips for implantable BCI devices.

ACKNOWLEDGMENTS

This work was partly supported by grants from the China Brain Project (2021ZD0200400), the Natural Science Foundation of China (61925603, 61906166, U1909202), and the Lingang Laboratory, Grant No.LG-QS-202202-04.

REFERENCES

- [1] D. Carlson and L. Carin, "Continuing progress of spike sorting in the era of big data," *Current Opinion in Neurobiology*, vol. 55, pp. 90–96, 2019.
- [2] B. C. Souza, V. Lopes-dos Santos, J. Bacelo, and A. B. Tort, "Spike sorting with gaussian mixture models," *Scientific Reports*, vol. 9, no. 1, pp. 1–14, 2019.
- [3] P. Yger, G. L. Spampinato, E. Esposito, B. Lefebvre, S. Deny, C. Gardella, M. Stimberg, F. Jetter, G. Zeck, S. Picaud, J. Duebel, and O. Marre, "A spike sorting toolbox for up to thousands of electrodes validated with ground truth recordings in vitro and in vivo," *eLife*, vol. 7, pp. 1–23, 2018.
- [4] L. Huang, L. Gan, and B. W. K. Ling, "A Unified Optimization Model of Feature Extraction and Clustering for Spike Sorting," *IEEE Transactions on Neural Systems and Rehabilitation Engineering*, vol. 29, pp. 750–759, 2021.
- [5] U. Rutishauser, E. M. Schuman, and A. N. Mamelak, "Online detection and sorting of extracellularly recorded action potentials in human medial temporal lobe recordings, in vivo," *Journal of Neuroscience Methods*, vol. 154, no. 1–2, pp. 204–224, 2006.
- [6] M. Pachitariu, N. Steinmetz, S. Kadir, M. Carandini, and H. Kenneth D., "Kilosort: realtime spike-sorting for extracellular electrophysiology with hundreds of channels," *bioRxiv*, p. 061481, 2016.
- [7] C. Rossant, S. N. Kadir, D. F. Goodman, J. Schulman, M. L. Hunter, A. B. Saleem, A. Grosmark, M. Belluscio, G. H. Denfield, A. S. Ecker, A. S. Tolias, S. Solomon, G. Buzski, M. Carandini, and K. D. Harris, "Spike sorting for large, dense electrode arrays," *Nature Neuroscience*, vol. 19, no. 4, pp. 634–641, 2016.
- [8] J. E. Chung, J. F. Magland, A. H. Barnett, V. M. Tolosa, A. C. Tooker, K. Y. Lee, K. G. Shah, S. H. Felix, L. M. Frank, and L. F. Greengard, "A Fully Automated Approach to Spike Sorting," *Neuron*, vol. 95, no. 6, pp. 1381–1394.e6, 2017. [Online]. Available: <https://doi.org/10.1016/j.neuron.2017.08.030>
- [9] G. Hilgen, M. Sorbaro, S. Pirmoradian, J.-O. Muthmann, I. E. Kepiro, S. Ullo, C. J. Ramirez, A. Puente Encinas, A. Maccione, L. Berdondini, V. Murino, D. Sona, F. Cella Zanacchi, E. Sernagor, and M. H. Hennig, "Unsupervised spike sorting for large-scale, high-density multielectrode arrays," *Cell Reports*, vol. 18, no. 10, pp. 2521–2532, 2017. [Online]. Available: <https://www.sciencedirect.com/science/article/pii/S221112471730236X>
- [10] F. J. Chaure, H. G. Rey, and R. Quiñ Quiroga, "A novel and fully automatic spike-sorting implementation with variable number of features," *Journal of Neurophysiology*, vol. 120, no. 4, pp. 1859–1871, 2018.
- [11] J. J. Jun, N. A. Steinmetz, J. H. Siegle, D. J. Denman, M. Bauza, B. Barbarits, A. K. Lee, C. A. Anastassiou, A. Andrei, Ç. Aydın *et al.*, "Fully integrated silicon probes for high-density recording of neural activity," *Nature*, vol. 551, no. 7679, pp. 232–236, 2017.
- [12] R. Diggelmann, M. Fiscella, A. Hierlemann, and F. Franke, "Automatic spike sorting for high-density microelectrode arrays," *Journal of Neurophysiology*, vol. 120, no. 6, pp. 3155–3171, 2018, pMID: 30207864. [Online]. Available: <https://doi.org/10.1152/jn.00803.2017>
- [13] N. A. Steinmetz, C. Aydın, A. Lebedeva, M. Okun, M. Pachitariu, M. Bauza, M. Beau, J. Bhagat, C. Böhm, M. Broux, S. Chen, J. Colonell, R. J. Gardner, B. Karsh, F. Kloosterman, D. Kostadinov, C. Mora-Lopez, J. O'Callaghan, J. Park, J. Putzeys, B. Sauerbrei, R. J. J. van Daal, A. Z. Volla, S. Wang, M. Welkenhuysen, Z. Ye, J. T. Dudman, B. Dutta, A. W. Hantman, K. D. Harris, A. K. Lee, E. I. Moser, J. O'Keefe, A. Renart, K. Svoboda, M. Häusser, S. Haesler, M. Carandini, and T. D. Harris, "Neuropixels 2.0: A miniaturized high-density probe for stable, long-term brain recordings," *Science*, vol. 372, no. 6539, p. eabf4588, 2021. [Online]. Available: <https://www.science.org/doi/abs/10.1126/science.abf4588>
- [14] R. Q. Quiroga, Z. Nadasdy, and Y. Ben-Shaul, "Unsupervised Spike Detection and Sorting with Wavelets and Superparamagnetic Clustering," *Neural Computation*, vol. 16, no. 8, pp. 1661–1687, aug 2004. [Online]. Available: <https://direct.mit.edu/neco/article/16/8/1661-1687/6903>
- [15] K. H. Kim and S. J. Kim, "A wavelet-based method for action potential detection from extracellular neural signal recording with low signal-to-noise ratio," *IEEE Transactions on Biomedical Engineering*, vol. 50, no. 8, pp. 999–1011, 2003.
- [16] R. J. Brychta, S. Tuntrakool, M. Appalsamy, N. R. Keller, D. Robertson, R. G. Shavi, and A. Diedrich, "Wavelet methods for spike detection in mouse renal sympathetic nerve activity," *IEEE Transactions on Biomedical Engineering*, vol. 54, no. 1, pp. 82–93, 2007.
- [17] J. Boussard, E. Varol, H. D. Lee, N. Dethle, and L. Paninski, "Three-dimensional spike localization and improved motion correction for neuropixels recordings," *Advances in Neural Information Processing Systems*, vol. 34, pp. 22095–22105, 2021.
- [18] H. Hazan, D. Saunders, D. T. Sanghavi, H. Siegelmann, and R. Kozma, "Unsupervised learning with self-organizing spiking neural networks," in *2018 International Joint Conference on Neural Networks (IJCNN)*, 2018, pp. 1–6.
- [19] D. Gutierrez-Galan, J. P. Dominguez-Morales, F. Perez-Peña, A. Jimenez-Fernandez, and A. Linares-Barranco, "Neuropod: A real-time neuromorphic spiking cpg applied to robotics," *Neurocomputing*, vol. 381, pp. 10–19, 2020. [Online]. Available: <https://www.sciencedirect.com/science/article/pii/S0925232129315644>
- [20] N. Imam and T. A. Cleland, "Rapid online learning and robust recall in a neuromorphic olfactory circuit," *Nature Machine Intelligence*, vol. 2, no. 3, pp. 181–191, Mar. 2020. [Online]. Available: <https://doi.org/10.1038/s42256-020-0159-4>
- [21] B. Chakraborty, X. She, and S. Mukhopadhyay, "A fully spiking hybrid neural network for energy-efficient object detection," *IEEE Transactions on Image Processing*, vol. 30, pp. 9014–9029, 2021.
- [22] C. M. Parameshwara, S. Li, C. Fermüller, N. J. Sanket, M. S. Evanusa, and Y. Aloimonos, "Spikems: Deep spiking neural network for motion segmentation," in *2021 IEEE/RSJ International Conference on Intelligent Robots and Systems (IROS)*, 2021, pp. 3414–3420.
- [23] T. Wu, W. Zhao, E. Keefer, and Z. Yang, "Deep compressive autoencoder for action potential compression in large-scale neural recording," *Journal of Neural Engineering*, vol. 15, no. 6, p. 066019, oct 2018. [Online]. Available: <https://dx.doi.org/10.1088/1741-2552/aae18d>
- [24] T. Wu, A. Rátkai, K. Schlett, L. Grand, and Z. Yang, "Learning to sort: Few-shot spike sorting with adversarial representation learning," in *2019 41st Annual International Conference of the IEEE Engineering in Medicine and Biology Society (EMBC)*, 2019, pp. 713–716.
- [25] M. S. ur Rehman, R. Lienkämper, Y. Parpaley, J. Wellmer, C. Liu, B. Lee, S. Kellis, R. Andersen, I. Iossifidis, T. Glasmachers, and C. Klaes, "Spikedeeper: a deep-learning based method for

- detection of neural spiking activity,” *Journal of Neural Engineering*, vol. 16, no. 5, p. 056003, jul 2019. [Online]. Available: <https://dx.doi.org/10.1088/1741-2552/ab1e63>
- [26] M. Rácz, C. Liber, E. Németh, R. Fiáth, J. Rokai, I. Harmati, I. Ulbert, and G. Márton, “Spike detection and sorting with deep learning,” *Journal of Neural Engineering*, vol. 17, no. 1, p. 016038, jan 2020. [Online]. Available: <https://dx.doi.org/10.1088/1741-2552/ab4896>
- [27] J. Rokai, M. Rácz, R. Fiáth, I. Ulbert, and G. Márton, “Elvisort: encoding latent variables for instant sorting, an artificial intelligence-based end-to-end solution,” *Journal of Neural Engineering*, vol. 18, no. 4, p. 046033, apr 2021. [Online]. Available: <https://dx.doi.org/10.1088/1741-2552/abf521>
- [28] J. Wouters, F. Kloosterman, and A. Bertrand, “A data-driven spike sorting feature map for resolving spike overlap in the feature space,” *Journal of Neural Engineering*, vol. 18, no. 4, p. 0460a7, jul 2021. [Online]. Available: <https://dx.doi.org/10.1088/1741-2552/ac0f4a>
- [29] J. Eom, I. Y. Park, S. Kim, H. Jang, S. Park, Y. Huh, and D. Hwang, “Deep-learned spike representations and sorting via an ensemble of auto-encoders,” *Neural Networks*, vol. 134, pp. 131–142, 2021. [Online]. Available: <https://www.sciencedirect.com/science/article/pii/S0893608020303944>
- [30] S. Mukhopadhyay and G. Ray, “A new interpretation of nonlinear energy operator and its efficacy in spike detection,” *IEEE Transactions on Biomedical Engineering*, vol. 45, no. 2, pp. 180–187, 1998.
- [31] S. Thorpe and J. Gautrais, “Rank order coding,” in *Computational neuroscience*. Springer, 1998, pp. 113–118.
- [32] S. Schliebs and N. Kasabov, “Evolving spiking neural network-a survey,” *Evolving Systems*, vol. 4, no. 2, pp. 87–98, jun 2013. [Online]. Available: <http://link.springer.com/10.1007/s12530-013-9074-9>
- [33] D. O. Hebb, “Drives and the cns (conceptual nervous system).” *Psychological Review*, vol. 62, no. 4, p. 243, 1955.
- [34] A. P. Buccino, C. L. Hurwitz, S. Garcia, J. Magland, J. H. Siegle, R. Hurwitz, and M. H. Hennig, “Spikeinterface, a unified framework for spike sorting,” *eLife*, vol. 9, pp. 1–24, 2020.
- [35] D. A. Adamos, E. K. Kosmidis, and G. Theophilidis, “Performance evaluation of pca-based spike sorting algorithms,” *Computer Methods and Programs in Biomedicine*, vol. 91, no. 3, pp. 232–244, 2008.
- [36] D. A. Henze, Z. Borhegyi, J. Csicsvari, A. Mamiya, K. D. Harris, and G. Buzsáki, “Intracellular features predicted by extracellular recordings in the hippocampus in vivo,” *Journal of Neurophysiology*, vol. 84, no. 1, pp. 390–400, 2000.
- [37] D. Henze, K. Harris, Z. Borhegyi, J. Csicsvari, A. Mamiya, H. Hirase, A. Sirota, and G. Buzsáki, “Simultaneous intracellular and extracellular recordings from hippocampus region ca1 of anesthetized rats,” *CRCNS.org*, 2009.
- [38] Y. Wang, F. Wang, K. Xu, Q. Zhang, S. Zhang, and X. Zheng, “Neural control of a tracking task via attention-gated reinforcement learning for brain-machine interfaces,” *IEEE Transactions on Neural Systems and Rehabilitation Engineering*, vol. 23, no. 3, pp. 458–467, 2014.
- [39] H. G. Rey, C. Pedreira, and R. Quiñero, “Past, present and future of spike sorting techniques,” *Brain Research Bulletin*, vol. 119, pp. 106–117, 2015. [Online]. Available: <http://dx.doi.org/10.1016/j.brainresbull.2015.04.007>
- [40] A. P. Buccino, S. Garcia, P. Yger, and C. D. Recherche, “Spike sorting : new trends and challenges of the era of high-density probes,” *OSF Preprints*, no. January 7, pp. 1–20, 2022.
- [41] Z. S. Zaghloul and M. Bayoumi, “Adaptive neural matching online spike sorting vlsi chip design for wireless bci implants,” in *2015 IEEE International Conference on Acoustics, Speech and Signal Processing (ICASSP)*. IEEE, 2015, pp. 977–981.
- [42] —, “Implementable spike sorting techniques for vlsi wireless bci/bmi implants: A survey,” in *The 5th International Conference on Energy Aware Computing Systems & Applications*. IEEE, 2015, pp. 1–4.
- [43] Y. Cao, Y. Chen, and D. Khosla, “Spiking Deep Convolutional Neural Networks for Energy-Efficient Object Recognition,” *International Journal of Computer Vision*, vol. 113, no. 1, pp. 54–66, 2015. [Online]. Available: <http://dx.doi.org/10.1007/s11263-014-0788-3>
- [44] M. Davies, N. Srinivasa, T.-H. Lin, G. Chinya, Y. Cao, S. H. Choday, G. Dimou, P. Joshi, N. Imam, S. Jain *et al.*, “Loihi: A neuromorphic manycore processor with on-chip learning,” *IEEE Micro*, vol. 38, no. 1, pp. 82–99, 2018.
- [45] J. V. Arthur, P. A. Merolla, F. Akopyan, R. Alvarez, A. Cassidy, S. Chandra, S. K. Esser, N. Imam, W. Risk, D. B. D. Rubin, R. Manohar, and D. S. Modha, “Building block of a programmable neuromorphic substrate: A digital neurosynaptic core,” in *the 2012 International Joint Conference on Neural Networks (IJCNN)*, 2012, pp. 1–8.
- [46] T. Werner, E. Vianello, O. Bichler, D. Garbin, D. Cattaert, B. Yvert, B. D. Salvo, and L. Perniola, “Spiking neural networks based on OxRAM synapses for real-time unsupervised spike sorting,” *Frontiers in Neuroscience*, vol. 10, no. NOV, pp. 1–12, 2016.
- [47] M. Bernert and B. Yvert, “An Attention-Based Spiking Neural Network for Unsupervised Spike-Sorting,” *International Journal of Neural Systems*, vol. 29, no. 8, pp. 1–19, 2019.